Environmental Technology & Innovation 30 (2023) 103133

Contents lists available at ScienceDirect

Environmental Technology & Innovation

journal homepage: www.elsevier.com/locate/eti

Highly efficient photodegradation of methylene blue by a composite photocatalyst of bismuth nanoparticles on silicon nanowires

Mariem Naffeti [a,b,c], Mohamed Ali Zaïbi [a,c], Chayma Nefzi [d], Alejandro Vidal García-Arias [b], Radhouane Chtourou [a], Pablo Aitor Postigo [b,e,*]

[a] Laboratory of Nanomaterials and Systems for Renewable Energies (LaNSER), Research and Technology Center of Energy, Techno-Park Borj-Cedria, Bp 95, 2050 Hammam-Lif, Tunis, Tunisia
[b] Instituto de Micro y Nanotecnología, IMN-CNM, CSIC (CEI UAM+CSIC) Isaac Newton, 8, E-28760 Tres Cantos, Madrid, Spain
[c] Tunis University—National High School of Engineering of Tunis, 5 Av Taha Hussein, 1008 Tunis, Tunisia
[d] University of Tunis El Manar, Faculty of Science of Tunis, Department of Physics, LR99ES13, Physics laboratory of the Condensed Matter (LPMC), 2092, Tunis, Tunisia
[e] The Institute of Optics, University of Rochester, Rochester, NY 14627, USA

ARTICLE INFO

Article history:
Received 3 January 2023
Received in revised form 14 March 2023
Accepted 29 March 2023
Available online 5 April 2023

Keywords:
Si nanowires
Bi nanoparticles
Optical properties
Methylene blue photocatalytic degradation
UV irradiation
Solar irradiation

ABSTRACT

When synthetic dyes are used to embellish the world, the wastewater holding these hazardous materials is wantonly released into the biosphere. Appropriate treatment for such effluents is thereby indispensable. In this context, the present study was conducted to fabricate an eco-friendly, cost-effective and new bismuth modified silicon nanowires (Bi@SiNWs)-based photocatalysts toward superior photocatalytic degradation of methylene blue (MB) dye under both UV and solar irradiations. SiNWs were synthesized by silver-assisted chemical etching while Bi nanoparticles were anchored onto the NWs via thermal evaporation. By assessing the morphology, elemental composition, structure and crystallinity characteristics, these Bi@SiNWs nanocomposites are systematically identified. Extensive investigations of blank SiNWs and Bi@SiNWs optical properties — reflectance, transmittance, absorption coefficient, absorbance and optical band-gap — are presented. Near-perfect absorbance above 97%, over the visible wavelength region, has been achieved owing to the synergistic effect of Bi decoration on SiNWs. Accordingly, Bi@SiNWs showed remarkable photocatalytic ability for the degradation of MB up to 44% and 89% under UV and solar irradiation, respectively, only within 120 min. Repeated cycle runs revealed that the Bi@SiNWs composite photocatalyst exhibits strong reusability and photo-stability. Lastly, we will thoroughly provide the plausible mechanism for the photocatalytic degradation of MB over Bi@SiNWs. Our outcomes validate the potent role of Bi@SiNWs photocatalysts for effective environmental remediation.

1. Introduction

Over the past years, the continuous growth of the world's population conjoined with urbanization and industrialization has led to rising demand for energy, materials, and chemicals (Rani et al., 2020). The discharge of large quantities of undesirable wastes from many artificial sources into the environment is inevitably accompanied by lower quality of

* Corresponding author.
E-mail addresses: naffeti.mariam@gmail.com (M. Naffeti), Pabloaitor.postigo@imm.cnm.csic.es (P.A. Postigo).

https://doi.org/10.1016/j.eti.2023.103133

many ecosystems, mainly aquatic habitats. While the textile, paper, plastic, food processing and cosmetics industries, play essential roles in the global economy, they also serve as the largest sources of environmental pollution (Wang et al., 2021). Accurately, myriad volumes of potable water combined with a wide range of hazardous synthetic dyes are utilized at various manufacturing stages. When the polluted water streams go into lakes and rivers, the pollutants threaten the aquatic resources, and thus the entire ecosystem including plants, animals, and humans. Because they contain high concentrations of organic and inorganic compounds, these effluents, or their degradation substances cause serious water-borne diseases such as skin irritation, nausea, vomiting, diarrhea, congenital malformation, and even cancer (Hu et al., 2018; Shi et al., 2020). One example of the hazard effluents is Methylene blue (MB), a common cationic dye and is non-degradable because of its complex structure and can therefore cause long-term pollution (Mehwish et al., 2021). Thus, effectively eradicating pollutants from wastewater is urgently needed and paramount to protect the environment and the sustainable development of those industrial sectors.

So far, many conventional treatments such as physical (adsorption, filtration, ion exchange, sedimentation) (Samsami et al., 2020), chemical (coagulation, flocculation, electrochemical) (Liang et al., 2014) and biological approaches (bioaccumulation, bio-sorption, biodegradation) (Kong et al., 2019) have been established. However, the practical use of these techniques is generally restricted as their applications are associated with complex and/or time-consuming processes, expensive equipment and/or chemicals, and the production of wastes and by-products where some of which can be more harmful and toxic than the primary pollutants (Al-Mamun et al., 2019; Rosu et al., 2017). Therefore, the development of better technologies for water treatment and environmental remediation has become mandatory. Indeed, heterogeneous photocatalytic oxidation, one of the Advanced Oxidation Processes (AOP), has proved to be an easy, cost-effective, environmentally friendly, and proper means to water disinfection (Rani et al., 2020; Al-Mamun et al., 2019; Naama et al., 2016; Saratale et al., 2020). In AOP, the photocatalyst absorbs the light energy (solar, UV and/or visible light irradiation), and subsequently degrades the hazardous compounds into harmless molecules through the formation of highly reactive chemical species such as hydroxyl radicals (Rani et al., 2020; Al-Mamun et al., 2019; Naama et al., 2016; Saratale et al., 2020). Certainly, using solar light is an optimal route to treat sewage due to its persistent energy and free of charge.

Various semiconductor materials, including ZnO, TiO_2, WO_3, SnO_2, Fe_2O_3, and others, have been widely used as heterogeneous photocatalysts for degrading organic pollutants to "green" species (Shi et al., 2020; Rosu et al., 2017; Tang et al., 2018; Theerthagiri et al., 2018; Babu et al., 2018). Nevertheless, two are the well-known drawbacks of these latter: the fast recombination rate of electron–hole pairs and thus low quantum yield; and the wide band-gap which can only absorb UV light that accounts for less than 5% of all solar radiation, thus limiting its practical application (Shi et al., 2020; Rosu et al., 2017; Tang et al., 2018; Theerthagiri et al., 2018; Babu et al., 2018). Other species, like CdS, suffer from toxicity and photocorrosion (Shen and Guo, 2008). In contrast, one-dimensional silicon nanowires are regarded as a highly effective option for photocatalytic treatment since, apart from being abundant, non-toxic, low-cost and having enormous specific surface area, they exhibit a wide optical adsorption range and a high optical absorption efficiency (Naffeti et al., 2020a; Brahiti et al., 2018; Lian et al., 2011). Recently, SiNWs have been shown to have relatively high photocatalytic activity to remove different types of pollutants such as tartrazine, methyl orange, methyl red, rhodamine B, rhodamine 6G, rose bengal, phenol and benzyl alcohol besides to methylene blue (Naama et al., 2016; Brahiti et al., 2018; Lian et al., 2011; Ghosh et al., 2018; Ghosh and Giri, 2016). In fact, SiNWs often evince defects and dangling bonds created during the elaboration process and the spontaneous oxidation in ambient atmosphere as well as to the recombination activities (Naffeti et al., 2020b). This thereby limits the overall quantum efficiency of the photocatalyst.

One of the most fruitful strategies to address the drawbacks is SiNWs surface passivation via the introduction of metal nanoparticles (MNPs). The major advantages of using MNPs with SiNWs as photocatalysts are (i) the higher absorption due to the surface plasmon resonance (SPR) effect of metals; (ii) the high work function of metals facilitates the electron transfer from SiNWs to metal in the Schottky junction, which remarkably reduces the recombination of photogenerated electron–hole pairs and (iii) the increase of the specific surface toward extending the photo-response and photoactivity. For instance, an enhanced UV-light-driven photocatalytic efficiency when increasing the deposition time of AuNPs was recently reported (Brahiti et al., 2018). Ghosh et al. showed significantly enhanced photocatalytic activity of SiNWs over 98% within 200 min after AgNPs were loaded onto them (Ghosh et al., 2018). Moreover, Wang et al. revealed that Pt modified silicon carbide nanowires (Pt/SiCNWs) demonstrate more than 88% improved photocatalytic activity for water splitting compared with the blank SiCNWs (Wang et al., 2014). Numerous other nanoscale metals have been loaded on SiNWs for photocatalytic purposes e.g., Pd; Cu; Ni; and even bimetal nanoparticles, e.g., Au–Ag, Au–Pd, and Pd–Ni (Naama et al., 2016; Brahiti et al., 2018; Ghosh et al., 2018; Ghosh and Giri, 2016; Liao et al., 2015; Hammouche et al., 2021).

Afar of the expensive metals and to the best of our knowledge, bismuth (Bi), the so-called "wonder metal", is an attractive and practical option that has not been unveiled yet for the decoration of SiNWs toward enhanced photocatalytic performance. It is one of the post-transition metals, abundant, environment-friendly, good absorber, and bestowed plasmonic properties (Sun et al., 2014; Benabdallah et al., 2018; Dong et al., 2014). On the other hand, a number of ongoing studies reveal evidence of negative effects of Bi on soil enzymatic activity and soil bacteria, plants, earthworms, and humans (Sudina et al., 2021; Pelepenko et al., 2022). These latter depend on the concentration of bismuth in the soil and the period of time after the start of contamination. Herein, Bi nanoparticles were loaded onto the SiNWs via thermal evaporation and in tiny quantities. Once the adsorption is fulfilled, the reactivity of Bi@SiNWs nanocomposite is of the decomposition type of MB and not a reaction of the BiNPs with MB or water, which will be released into nature. Therefore, there is no fear of contamination of the environment and subsequently the health of individuals.

The present study was conducted to prepare Bi-modified SiNWs nanocomposite as new UV and solar light active photocatalyst toward efficient degradation of MB dye. The resulting Bi@SiNWs were characterized using SEM, EDX, DRX, TEM, UV–Vis and XPS analysis. Then, we studied their photocatalytic activity on MB removal. We also assessed pure MB dyes and unmodified SiNWs photocatalytic performance for comparison. Besides, the cycling capability, photocatalysis mechanism and reactions kinetics of MB decomposition, are investigated thoroughly. Overall, the Bi@SiNWs potential in MB detoxification was explored.

2. Materials and methods

2.1. Reagents and materials

The primary material used in this work is single-side polished silicon wafers, (100) oriented, p-type boron doped, with a resistivity of 1–20 Ω cm and a thickness of 500 μm purchased from Siltronics. The chemical reagents used for the cleaning, etching process, and sample surface modification, such as acetone, ethanol, isopropanol, hydrofluoric acid (HF, 40%), silver nitrate ($AgNO_3$), hydrogen peroxide (H_2O_2, 35%), nitric acid (HNO_3, 65%), and bismuth (Bi, 99%), were obtained from Sigma-Aldrich. Methylene blue (MB, ≥ 95%, Sigma-Aldrich) was taken as a reference dye for investigating the photocatalysis activities and was used without further purifications. Deionized water (18 MΩ) was used for all the experiments.

2.2. Preparation of SiNWs

SiNWs were synthesized by the two-step Ag-assisted chemical etching (2-Ag-ACE) method as shown in Figure S1. The silicon wafers were first cleaned by ultra-sonication in acetone, ethanol, isopropanol, and deionized water (DI) for 15 min each. Cleaned substrates were then immersed in diluted HF for 3 min to remove the native oxide. The latter were dipped for 1 min into an aqueous solution composed of 4.8 M HF and 0.035 M $AgNO_3$ to deposit silver nanoparticles (AgNPs) on Si. After a proper rinsing, the wafers were immersed in an etching bath containing 4.8 M HF and 0.5 M H_2O_2 at room temperature for 20 min. The resulting samples were rinsed with DI and then soaked in nitric acid for 15 min to ensure the removal of Ag nanoparticles and dendrites. Finally, the as-formed homogeneous black silicon nanowires were rinsed with DI and dried under a gentle stream of nitrogen.

2.3. Preparation of BiNPs@SiNWs composites

For the preparation of BiNPs@SiNWs composites, a simple thermal evaporation technique was adopted using high purity metal bismuth powder as source material. Before deposition, the chamber and tungsten boat were minutely cleaned with acetone. Then, the Bi was set onto the cleaned tungsten boat and the chamber was evacuated to a high vacuum. At a vacuum of about 10^{-5} torr, the Bi was indirectly subjected to heat treatment by the heating of the tungsten boat, and the evaporation started to occur with a rate of 0.5 As^{-1}. Finally, ∼20 nm thick Bi was deposited, which was monitored via a quartz crystal microbalance. The resulting BiNPs@SiNWs composites were ultimately annealed at 100 °C for a few minutes under a nitrogen atmosphere.

2.4. Photocatalytic activity measurement

Methylene blue dye was used in this work as model of degraded material to assess the photocatalysis performance of the as-fabricated samples. The MB irradiation was carried out under various conditions as follows:

(i) Direct UV light irradiation without sample
(ii) In the presence of silicon nanowires under UV light irradiation
(iii) In the presence of silicon nanowires coated with Bi nanoparticles under UV light irradiation
(iv) Direct natural sunlight irradiation without sample
(v) In the presence of silicon nanowires under natural sunlight irradiation
(vi) In the presence of silicon nanowires coated with Bi nanoparticles under natural sunlight irradiation

Initially, MB aqueous solution with a concentration of 10^{-5} M was prepared by dissolving 5 mg of MB powder in deionized water under a magnetic stirring at room temperature for a few minutes. After that and before irradiation, samples were placed in glass bottles containing 20 ml of aqueous dye solution each. They were kept in dark for 30 min under normal atmospheric conditions in order to establish adsorption–desorption equilibrium between the catalyst surface and the dye. For experiments under UV-irradiation, a UV-C tube lamp (55 W, length 90 cm, diameter 2, 6 cm), model G55T8 (Philips) was used as the irradiation source ($\lambda = 254$ nm) located in a closed chamber. The distance from the light source to the samples was 30 cm. On the other hand, investigations under natural sunlight were performed in an open air environment from 11 a.m. to 2 p.m. in May at latitude 36° 50′ North and longitude 10° 14′ East in Tunis, Tunisia (average solar irradiance 5.5 kWh/m^2/Day, https://nsrdb.nrel.gov/data-sets/international-data). The MB solution was sampled every 20 min, and the concentration of MB was determined spectrophotometrically by monitoring the absorption peak at 664 nm.

2.5. Characterizations

Scanning Electron Microscopy (SEM) images were obtained using a FEI Varios 460 and Energy Dispersive X-ray spectra (EDX) were recorded using the SEM. X-ray diffraction (XRD) patterns of the produced materials were collected using an automated Bruker D8 advanced X-ray diffractometer (Bruker) with Cu Kα ($\lambda = 1.54$ Å) in the 2θ range of 20°–80°. Reflectance and transmittance measurements were recorded with UV–Vis–NIR spectrophotometer. Besides, the absorption spectra of methylene blue solutions were recorded using a Perkin Elmer Lambda 950 spectrophotometer. X-ray photoelectron spectroscopy (XPS) was conducted using a SPECS GmbH system. A Semilab WT-2000 PVN was employed for minority carrier lifetime mapping via the microwave photoconductivity decay (μPCD) technique ($\lambda = 905$ nm, F = 10 GHz). The surface wettability of the samples were investigated by water contact angle measurements using Drop Shape Analysis System type DSA100 (Kruss GmbH). The Fourier Transform Infra-Red (FTIR) spectra were taken using a Bruker IFS66v/s FTIR spectrometer.

3. Results and discussion

3.1. Morphology and structure

To have a good insight into the morphology and constitution of the elaborated nanostructures, SEM and EDX investigations were performed. Two-step Ag-ACE was introduced to fabricate the SiNWs which is a simple, reproducible, and low cost process using Ag catalysts in the HF/H_2O_2 etching agent. The 2-Ag-ACE begins by deposition of Ag nanoparticles onto the Si surface, and the Si directly beneath the deposited Ag is dissolved by the HF etchant, as depicted in Fig. 1a–b The EDX elemental spectra corroborate the presence of Si and Ag (Fig. 1.a). When the resulting nanostructure dipped into the HF/H_2O_2 etching solution, the AgNPs sink downwards vertically along the (100) direction in the pits thus formed, resulting in the SiNWs formation wrapped by dendrites (Fig. 1.d–e). The formation of Ag dendrites can be ascribed to AgNPs agglomeration during the extended etching time. EDX shows that these dendrites are composed of silver.

Once the sample is immersed in the HNO_3 aqueous solution, the recognizable SiNWs arrays can be observed where all the tree-like dendritic structures are removed. A plan view shown in Fig. 1.g indicates that the substrate surface was uniformly covered with nanowires which join together to form bundles through the attractive forces of Van der Walls (Naffeti et al., 2020b). The cross-section image, displayed in Fig. 1.h points out that the average length of the vertically aligned nanowires is approximately 3 μm. The SiNW arrays are covered with numerous porous structures — namely, silicon nanocrystals (SiNCs) — resulting from the lateral etching of NW side walls (Figure S2). One can note the SiNCs size were estimated in our antecedent work via an analytical model and were found to be less than 5 nm (Naffeti et al., 2020a). The average volume filling ratio (VFR) at the air/SiNW arrays was also determined. VFR is found equal to 0.45 at 20 min of etching time (Naffeti et al., 2020a). The corresponding EDX spectra of Fig. 1.i reveal that the SiNWs consist of silicon and oxygen. The detected small amount of oxygen is mainly due to the oxidation that occurred during the etching of the Si. Besides, there are no detectable Ag traces, confirming the complete removal of the silver nanoparticles and dendrites by nitric acid. It is noteworthy that an itemized elucidation of the mechanism and the chemical reactions occurring during the SiNWs fabrication process are communicated in our previous report (Naffeti et al., 2020a). Afterward, the SiNWs were capped with Bi nanoparticles. The latter are observed to be well dispersed along the whole SiNWs from the upper (Fig. 1.j) to the sidewall and bottom (Fig. 1.k) of the wires. Characteristic elemental peaks of Bi are well distinguished in the EDX spectra as shown in Fig. 1.l. The above findings are indicative the successful synthesis of Bi@SiNWs nanocomposite.

The crystal structure of the pure SiNWs and Bi-modified SiNWs were analyzed by XRD, and the results are illustrated in Fig. 2.a. SiNWs are predominantly (400)-oriented and still have excellent crystalline quality. Notice that one extra diffraction peak appears at 33°, presumably belonging to the Si (200) plane. Similar crystalline quality was obtained after Bi loading on SiNW arrays. In the XRD pattern of Bi@SiNWs, the characteristic diffraction peaks at 2θ values of 27° and 38° are matched well with the (012) and (104) crystal plane of Bi respectively (Gao et al., 2019; Ibrahim et al., 2019; Ensafi et al., 2017). This indicates crystalline bismuth formation, albeit that the diffraction peaks are weak.

Apart from the orientation and crystalline quality, the XRD calculates the crystallite size (D) of the deposited Bi nanoparticles using the Debye–Scherrer formula, as given in Eq. (1) (Liao et al., 2015):

$$D = \frac{k\lambda}{\beta \cos\theta} \tag{1}$$

where k is the Scherrer constant (∼0.9); $\lambda = 0.154$ nm denoting the wavelength of Cu–Kα X-ray radiation; β is the full width at half maximum (FWHM) of XRD peaks and θ is half of the Bragg angle.

According to the calculation from the (012) Bi intense diffraction peak, the average crystallite sizes of Bi are about 15 nm. This value is found to be concordant with the ones estimated via the high magnification SEM and TEM images (Fig. 2.b–c). Indeed, most of the nanoparticles are found to lie within 8∼24 nm in size. It is convenient to point out that the latter are quite smaller than the summit of aggregated BiNPs, particularly at the tips of the wires.

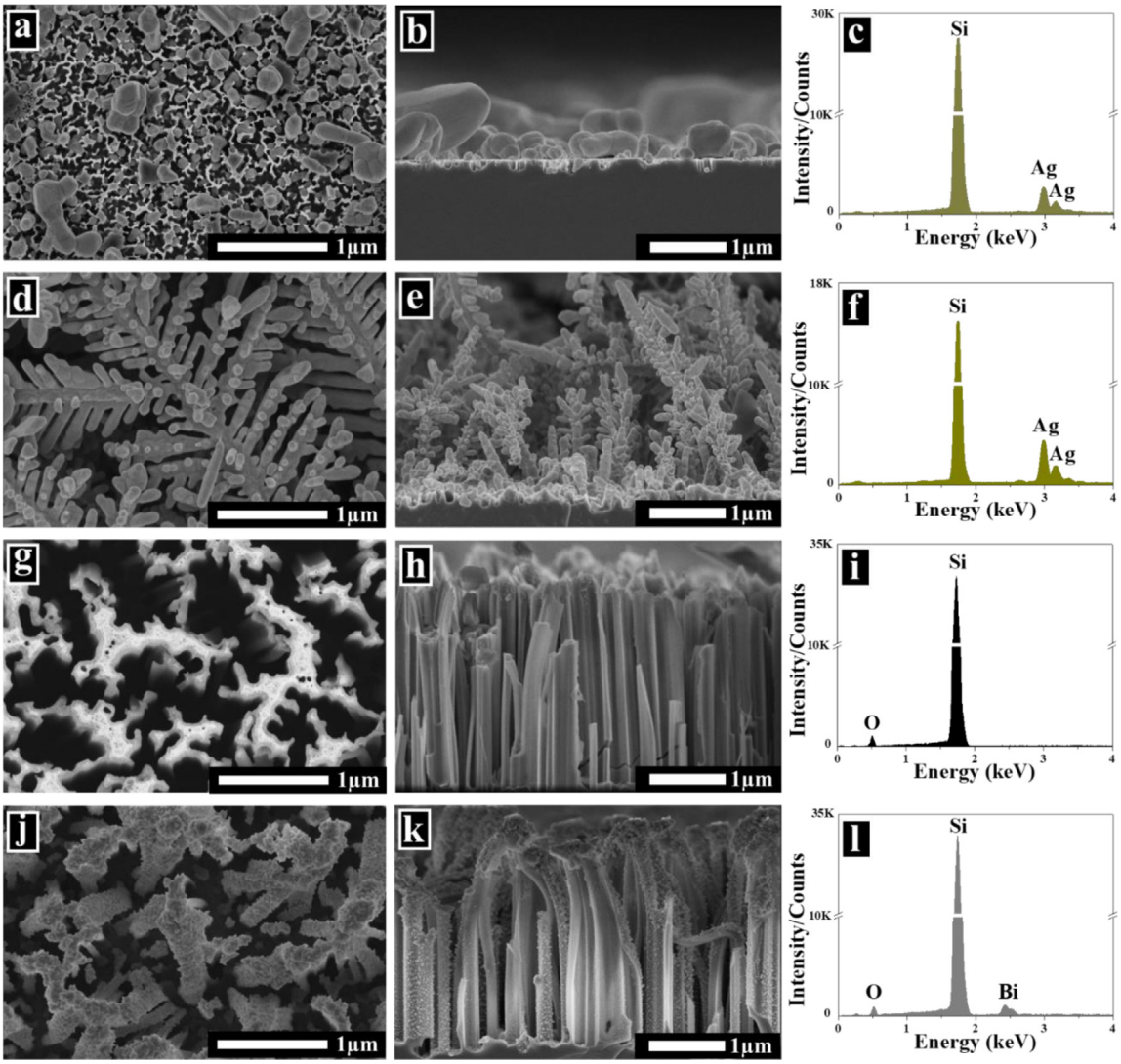

Fig. 1. Top view (a), cross-sectional view (b) and EDX spectra (c) of first step Ag-ACE; Top view (d), cross-sectional view (e) and EDX spectra (f) of second step Ag-ACE; Top view (g), cross-sectional view (h) and EDX spectra (i) of the resulted SiNWs; Top view (j), cross-sectional view (k) and EDX spectra (l) of Bi@SiNWs nanocomposite.

3.2. Optical properties

A key requirement for the developing of highly efficient photocatalysts for environmental applications, namely water purification, is the good management of their structural light scattering characteristics. In this vein, the optical properties of the untreated SiNW arrays and Bi-modified SiNWs composites were determined by reflectance (R) and transmittance (T) analysis. The spectral range of irradiation was in a range of UV to NIR from 250 to 2000 nm, which corresponds to the high spectral irradiance of sunlight. The reflectance spectra of the samples are shown in Fig. 3.a The untreated flat Si substrate exhibits high reflectance ranging from 78% to 25% in the UV–visible range. These relatively elevated values are due to the polished silicon surface and the absence of any incident light-trapping structures. The peak at 274 nm arises from the inter-band transitions of silicon (Naffeti et al., 2020a). The higher reflectance below the fundamental absorption bandgap (E_g) of silicon, i.e., in longer wavelengths, is due to the additional diffuse reflection from the back Si surface (Hung et al., 2011). After the formation of large-scale of vertical SiNWs, a strong suppression in the reflectance to about 6% in the above-bandgap spectral region occurred. Introducing BiNPs in the surface of SiNWs can further reduce the reflection loss of incident radiation, where the average reflectance reaches 3%. This highlights the effectiveness of Bi as an antireflection coating and in preserving the optical properties of SiNWs.

Fig. 3.b Compares the optical transmittance between the as-cited samples. One notices a discernible dependence of the transmittance on the spectral wavelength. Accurately, the average transmittance of the samples, including the one

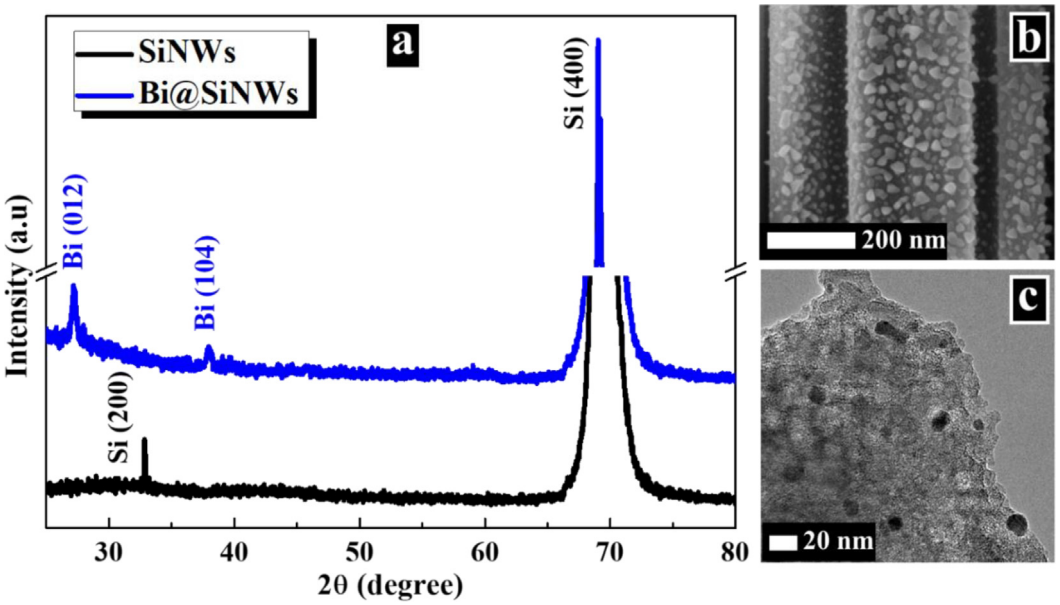

Fig. 2. XRD patterns of SiNWs and Bi@SiNWs (a), high magnification SEM (b) and TEM (c) images of Bi@SiNWs nanocomposite.

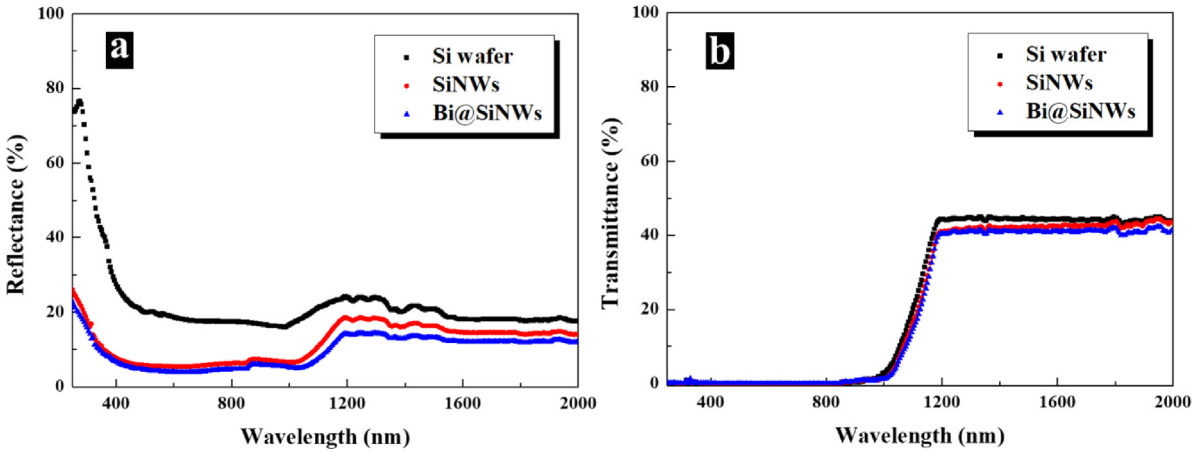

Fig. 3. Reflectance (a) and transmittance spectra (b) of bare silicon, SiNWs and Bi@SiNWs.

without the nanowires, was approximately zero in the above-bandgap spectral region (opaque region). In contrast, the transmittance in the near-infrared region (transparent region) was quite significant, reaching as high as 44%.

The very low reflectance and the zero transmittance of sole SiNWs and Bi@SiNWs indicate of high absorption. Indeed, high absorption coefficient (α) values are obtained, as readily seen from Fig. 4.a The α average values were calculated using the experimental values of T and R using Eq. (2) (Nefzi et al., 2019).

$$\alpha = \frac{-1}{e} Ln\left(\frac{T}{(1-R)^2}\right) \tag{2}$$

where e is the effective thickness as the length of the wires for SiNWs and Bi@SiNWs samples, whereas it is the wafer thickness for bare Si.

The Bi-rich SiNWs exhibit the highest α value of about 3.2×10^6 cm^{-1} in the visible range, which is topmost than those mentioned in previous works (Chaliyawala et al., 2017; Swain et al., 2011). Besides, the net internal absorption (A) is derived from the corresponding reflectance and transmittance according to R(%) + T(%) + A(%) = 100% (Fig. 4.b).

As expected, the Si nanowires exhibit strong optical absorbance with a broad spectral bandwidth of 400∼1000 nm, reaching as high as 95%. This can be attributed to two possible factors. First, the light trapping effect caused by the construction of the tapering nanowires' geometry, resulting in strong light confinement. Second, the gradual change in

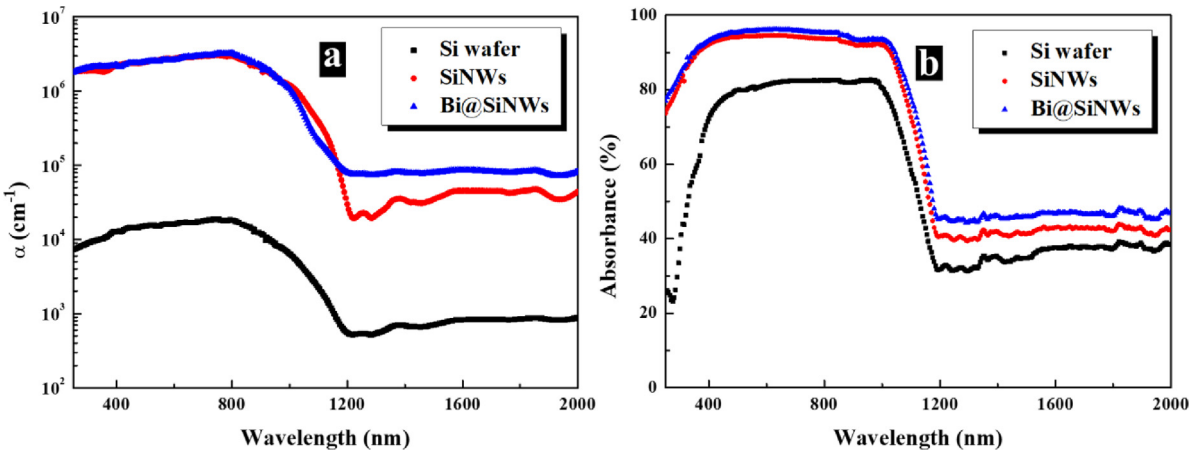

Fig. 4. Spectral absorption coefficient (α) as function of wavelength. (a) and absorbance spectra (b) of bare silicon, SiNWs and Bi@SiNWs.

the refractive index between air ($\eta_{air} \approx 1$) and SiNWs ($\eta_{SiNWs} \approx 1.95$). The value of η_{SiNWs} can be calculated by using the weighting formula as described in Eq. (3).

$$\eta SiNWs = FF \times \eta_{Si} + (1 - FF) \times \eta_{air} \tag{3}$$

where, FF is the filling factor of the nanowires which can be obtained by the surface morphology of SEM images using 'Image J' software (≈38%); η_{Si} is the refractive index of Si (≈3.5). Similar values have been obtained in literature (Hung et al., 2011; Chaliyawala et al., 2017). The high optical absorbance feature was evidenced by the black and dull appearance of SiNW surfaces to the naked eye. For Bi@SiNWs nanocomposite, the absorbed light is slightly increased to above 97% in the entire Si absorbing region. The latter comes from the effect of localized surface plasmonic resonance of semimetallic Bi, as well as the enhancement and lengthening of the optical path, thus increasing the capture ratio of photons (Naffeti et al., 2020b). After that, one can note that the decreased Absorbance above 1100 nm is owing to light scattering, where Bi@SiNWs nanocomposite own excellent light absorption in near-infrared (NIR) regions. This agrees with our previous report showing that Bi@SiNWs are NIR optically active materials (Naffeti et al., 2020b). A detailed comparison of the Absorbance in the UV, visible, and IR regions is summarized in Table S1.

Furthermore, the optical band gap (E_g) of all samples was estimated using Tauc's equation (Kashyap et al., 2021a,b):

$$\alpha h\nu = B(h\nu - E_g)^n \tag{4}$$

where h is Planck's constant (4.1357×10^{-15} eV s), ν is the light frequency, B is a constant, and n is a coefficient associated with the electronic transition (herein $n = 2$ for indirect allowed transitions). Fig. 5 shows the plots of $(\alpha h\nu)^2$ versus $h\nu$. The value of E_g is determined by extrapolating the straight-line portion of plots to the energy axis. The band gaps energy of sole SiNWs and compound Bi@SiNWs were found to be slightly higher than that of their bare silicon substrate counterpart. The deduced E_g is approximately 1.12 eV for the Si wafer and about 1.17 and 1.20 eV for SiNWs and Bi@SiNWs respectively. These findings agree with those of Hutagalung et al. (2017). Such band-gap widening is explained by (i) the quantum confinement (QC) effects that occur in low dimensional semiconductors possessing quantum sizes in the order of Bohr radius, and (ii) the large trapping light in textured silicon than that of bare Si (Naffeti et al., 2020a; Kashyap et al., 2021a; Hutagalung et al., 2017). Having confirmed the outstanding overall optical properties of SiNWs and particularly Bi@SiNWs, promising photodegradation performances are strongly expected to occur.

3.3. Photocatalytic properties

Evaluations of photocatalytic activity of unloaded SiNW arrays and Bi-loaded SiNWs composites were performed towards the degradation of MB dyes under UV and natural sunlight irradiation. Fig. 6 represents UV–Vis absorption spectra of pure MB dyes and their aqueous solution mixed with the catalyst samples as a function of irradiation time. The degradation of MB was assessed by following the gradual reduction of intensities of the main absorbance band centered at 664 nm with time.

Fig. 7.a–b manifests the MB degradation of the prepared photocatalysts. One can note that the decay of the dye molecule concentration as a function of exposure time decreases unevenly in an exponential form, implying an heteropolyaromatic linkage and destruction of a large quantity of the aromatic rings. The dye in wastewater is then converted in majority to inorganic simple, and non-toxic compounds, such as H_2O and CO_2, which are harmless.

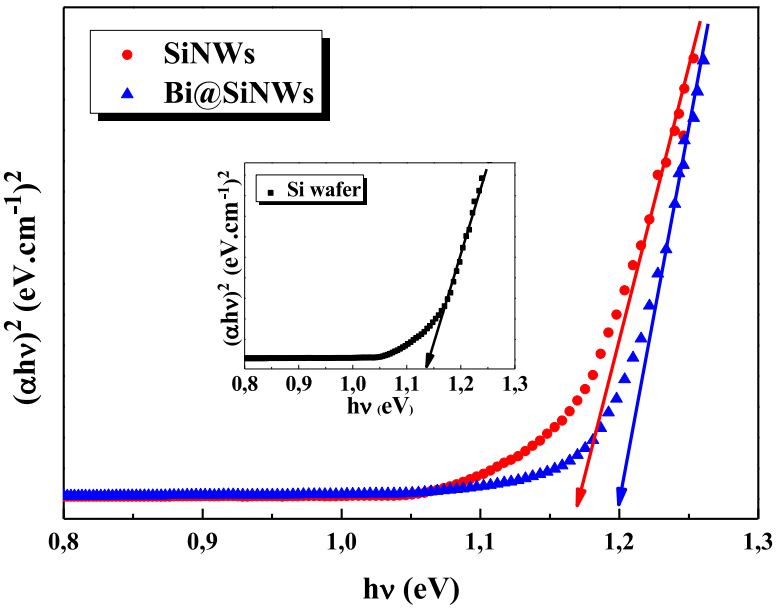

Fig. 5. Tauc's plot of bare Si, SiNWs and Bi@SiNWs.

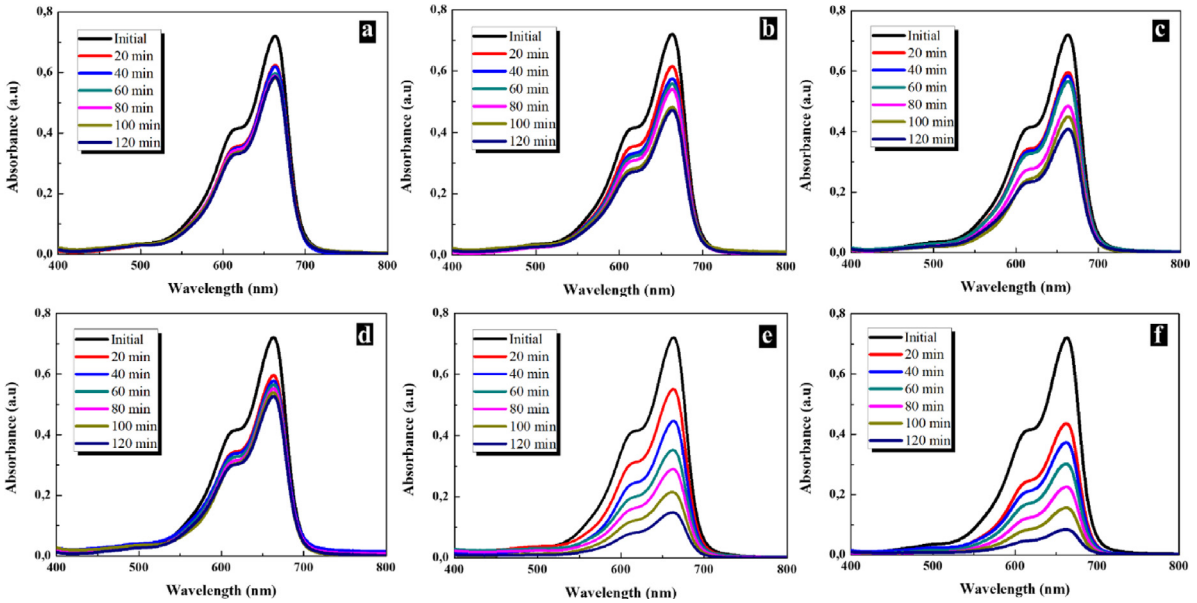

Fig. 6. UV–Vis absorption spectra. (a) MB dye without catalysis under UV light irradiation, (b) MB dye in the presence of SiNWs under UV light irradiation, (c) MB dye in the presence of Bi@SiNWs under UV light irradiation, (d) MB dye without catalysis under sunlight irradiation, (e) MB dye in the presence of SiNWs under sunlight irradiation and (f) MB dye in the presence of Bi@SiNWs under sunlight irradiation.

The degradation efficiency (D_{eff}) have been calculated using the equation given below (Liao et al., 2015):

$$Deff\ (\%) = \left(1 - \frac{C_t}{C_0}\right) \times 100 = \left(1 - \frac{A_t}{A_0}\right) \times 100 \tag{5}$$

where C_0 stands for the initial concentration of MB dye solution, and C_t represents the remaining concentration of MB at different time intervals. A_0 and A_t are the corresponding absorbance values of MB using Beer–Lambert's Law:

$$\frac{C_t}{C_0} = \frac{A_t}{A_0}$$

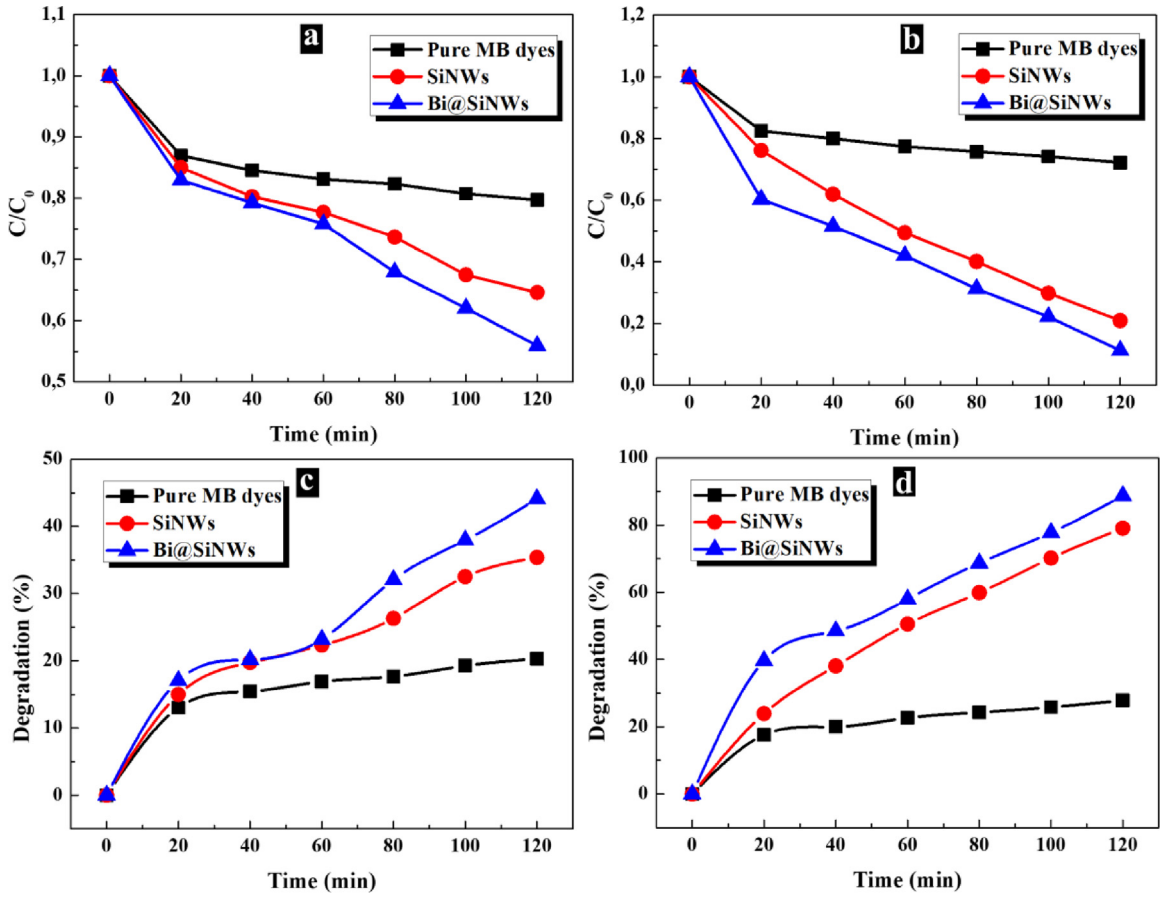

Fig. 7. Variation of MB concentration versus time without catalyst and in the presence of SiNWs and Bi@SiNWs under (a) UV and (b) sunlight irradiation. Corresponding degradation efficiency versus time under (c) UV light irradiation and (d) sunlight irradiation.

As shown in Fig. 7.c–d, the degradation efficiency of the dyes without catalysts are 20% and 27% after 120 min irradiation under UV and natural sunlight, respectively. This indicates a tiny self-photolysis of MB molecules under both conditions.

The second set of experiments involves the degradation of the dyes under UV and natural sunlight with the addition of SiNWs catalysts. Significant changes were observed in absorption spectrum of dyes; D_{eff} was also investigated and reached to about 35% (UV) and 78% (sunlight) for the same irradiation time (120 min). The photocatalytic activity of SiNWs can be ascribed to the following factors: (i) its high specific surface area, (ii) the quantum confinement effect and to (iii) the excitons generated within the self-grown silicon nanocrystals decorated SiNWs which are energetic enough to drive applicable photoelectrochemical reactions owing to its wide range of optical absorption (Naffeti et al., 2020a; Ghosh et al., 2018; Lin et al., 2018). This makes the SiNWs capable of initiating the oxidative process for dye degradation.

Notably, introducing Bi nanoparticles onto the surface of the SiNW arrays contributes to a noticeable improvement of the photocatalytic performance. Indeed, 44% and 89% of degradation were recorded after 120 min under UV and sun irradiation respectively. The boosting in the removal efficiency is associated with a synergetic effect between the plasmonic BiNPs co-catalyst and the pure photoactive SiNWs. Bismuth coating acts as charge mediator so that photogenerated electron–hole pairs could be sufficiently separated, thereby preventing partially their recombination. Indeed, a decrease of the effective surface recombination velocity (S_{eff}) is observed for Bi@SiNWs (2340 cm s^{-1}) comparing to the pure SiNWs (4098 cm s^{-1}). S_{eff} values has been calculated from the measured effective minority carrier lifetime (τ_{eff}) according to the following equation (Mallorquí et al., 2015):

$$Seff = \frac{w}{2\tau_{eff}} \tag{6}$$

where w is the wafer thickness. The τ_{eff} average values were extracted from the effective lifetime maps (Figure S3), where we took into account the middle of the samples for the most uniformity and homogeneity ($\approx$ 61 μs for SiNWs and $\approx$10.68 for Bi@SiNWs). Thus, the composite of Bi@SiNWs can efficiently generate a large number of active sites leading to absorb dye molecules and photons and hence contribute to an increase in the photocatalytic activity. Furthermore, Bi can serve as a protecting layer and effectively hinders self-oxidation of SiNWs during the photocatalytic process.

Aside from that, the wetting characteristics of SiNWs and Bi@SiNWs photocatalysts surfaces were analyzed, as shown in Figure S4. a. It was found that the Bi@SiNWs nanocomposite possessed the highly hydrophilic property with the contact angle of 52.3°, which was lower than SiNWs (contact angle = 67.6°). This can be attributed to the abundant hydroxyl groups existed in Bi@SiNWs surfaces as evidenced in FTIR spectra of Figure S4. b. This facilitate the contact of MB dye solutions with photocatalyst and thus might contribute to the improved photocatalytic performance.

To further unveil the photocatalytic kinetics, the involved reactions of dye degradation are examined with a basic kinetic model called Langmuir–Hinshelwood expressed by Eq. (7) (Hsiao et al., 2021):

$$Ln\left(\frac{C_t}{C_0}\right) = -Kt \tag{7}$$

This model narrates the rate constant (K) of the reaction for the photodegradation of MB dye molecules, which gives the chemical kinetics and follows the first-order kinetic model. The rate constant apprize the approximate number of dye molecules dissociated per second throughout the photodegradation process. Accordingly, the fitting results from experimental investigations are demonstrated in Fig. 8.a–b, where the highest rate constant is ascribed to Bi@SiNWs nanocomposite, validating the underlying kinetics for treating the MB dyes in the aqueous media under both illumination. All the experimental results, namely the calculated D_{eff}, K values and corresponding correlation coefficients (R^2) of the photocatalyst materials are summarized in Table S2.

On the other hand, enlightened by Fig. 8.c and Figure S5, two facts can be extracted: the first is that the photocatalytic performance of all the catalyst samples is higher under direct solar irradiation than with UV light. This observation is understandable owing to the materials' optical features as previously discussed (Table S1). Thus, light conditions significantly affect the performance of pollutant photodegradation, knowing that sunlight contains merely 5% UV light, 47% visible light and 48% infrared radiation. These latter photocatalysts can be excited to produce more electron hole-pairs under natural sunlight irradiation, which could result in efficient photocatalytic activity. This is advantageous as the solar irradiation is an abundant, renewable and free clean-energy resource. Higher decolorization efficiency under natural sunlight conditions than UV irradiation for different materials photocatalyst has been reported in the literature (Eskizeybek et al., 2012; García et al., 2016; Kiran et al., 2021). The second is the benefit impact of nanoscale dimension of Bi particles to increase the photocatalytic activity of SiNWs matrix highlighting its practical catalyst feature. Notably, these BiNPs in SiNWs-based photocatalytic systems are more favorable in terms of degradation efficiency or degradation time compared to previously reported photocatalytic nanocomposites based on SiNWs modified by other passivation materials. For instance, degradation efficiency of MB dyes up to 44,9%, 53% and 77% after 120 min of irradiation were recently reported for a ZnO/SiNWs composite, Cu_2O/SiNWs composite and Ternary ZnO/Cu2O/Si nanowire arrays, respectively (Hsiao et al., 2019). Tang et al. showed that the remaining concentrations of the MB dye were 34.2% and 63.7% for ZnO/ SiNW samples obtained by 15 times and 25 times of deposition cycles, respectively (Tang et al., 2018). In addition, Brahiti et al. showed a maximum degradation of MB about 88.32%, 91.93% and 97.23% for Pt-, Au- and Pd-modified SiNWs, respectively but for an irradiation time of 200 min (Brahiti et al., 2015).

Importantly, the stability and reusability of a photocatalyst is always considered as another important feature for its application, besides activity. Therefore, a cycling test was performed repetitively for four cycles for the MB degradation by the most efficient catalysts of SiNWs and Bi@SiNWs under solar irradiation (Figure S6). An almost similar decaying curves in terms of concentration of remaining dyes are presented after conducting the repeated tests for three times, reflecting the sound structural robusticity of such photocatalysts. It is noteworthy that a slight efficiency loss less than 6.7% for SiNWs and 7.4% for Bi@SiNWs occur for the last fourth cycle.

X-ray photoelectron spectroscopy analysis is investigated on SiNWs and Bi@SiNWs before (Figure S7.a–b) and after consecutive four cycles (Figure S7.c–d) of MB adsorption. The full survey spectrum were taken on the same scale of intensity (a.u) and binding energy (eV). It revealed the presence of Si2p, Si2s, C1s, O1s, Bi4d, and other Bi-related characteristic peaks without a record of any significant shift, though the nanostructures' dipping in the MB aqueous solution. This indicates that the phase and structure of the photocatalysts remained unchanged, which further confirms their stability. Nevertheless, one can see a remarkable decrease of the XPS peaks intensities after the adsorption of MB, denoting the interactions between adsorption functional groups of SiNWs and Bi@SiNWs and MB dye molecules that are loaded on their surface. This is consistent on the one hand with the modification in the surface morphology of SiNWs and Bi@SiNWs, where the MB dye molecules partially fill the gaps between the bunches of the Si wires; and on the other hand with the gradual fading from deep blue to light blue and almost colorless for SiNWs and Bi@SiNWs, respectively (insets Figure S7). All the aforementioned photocatalytic properties attest to the reliable and efficient peculiarities for the removal of MB dyes based on such photocatalysts. To our best knowledge, this is the first work shedding light on Bi@SiNWs nanocomposite as photocatalyst system. We anticipate that this developed photocatalyst will be a starting point for further research on water purification plans.

Let us now elucidate the possible photocatalysis mechanism involving Bi@SiNWs nanocomposite as a photocatalyst in the photodecomposition of MB (Figure S8). The Bi@SiNWs facilitates the degradation of MB via heterogeneous processes. The organic molecules are first adsorbed on the photocatalyst surfaces (denoted as path 1 in Figure S8), and then degradation reaction (path 2) occurs, without neglecting the fact that some organic contaminants can undergo direct photolysis (path 3). In reality, degradation reaction is the dominant process. It appears then reasonable to highlight the possible catalytically active species first. On the basis of numerous experimental studies, if the photoinduced electrons

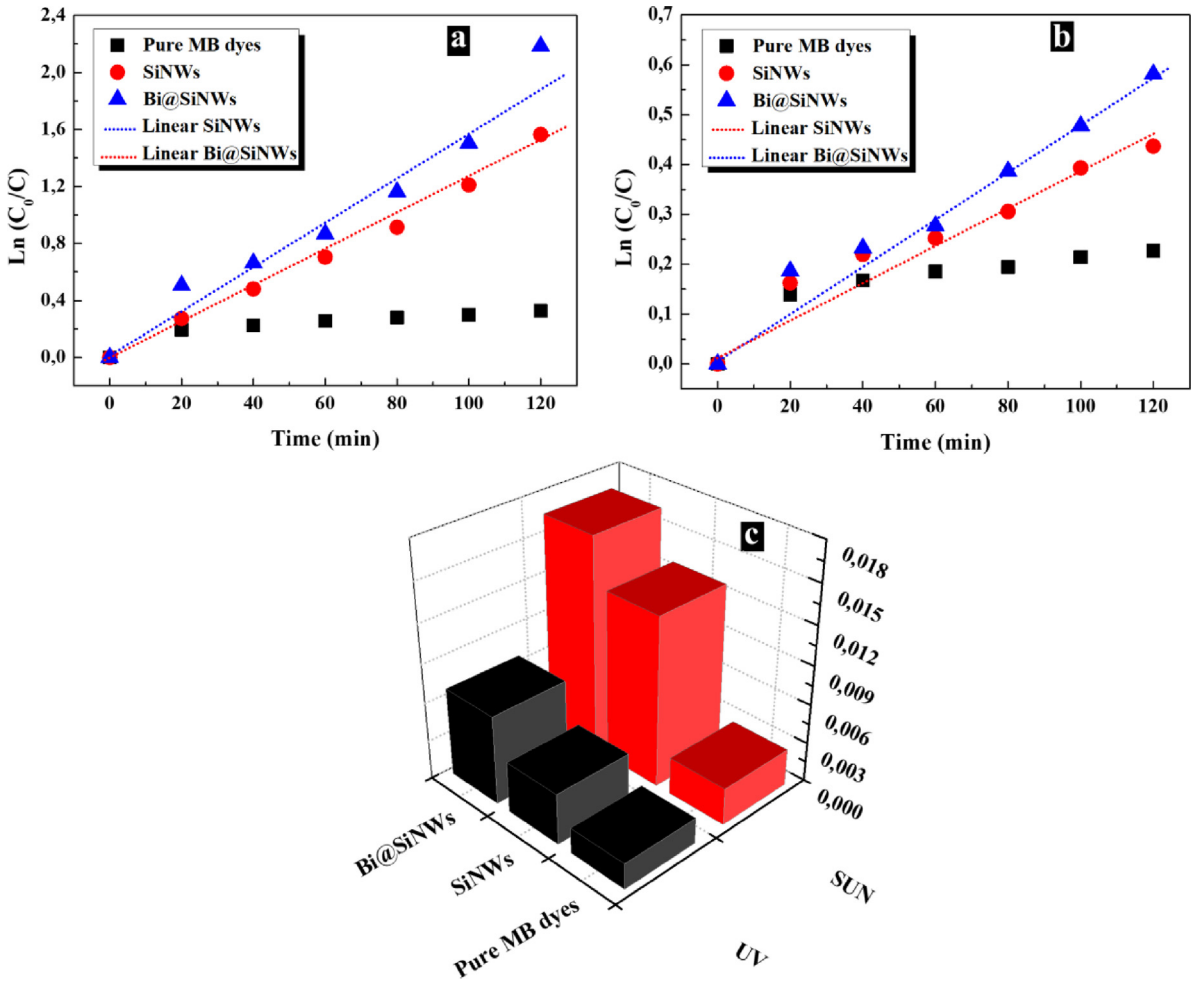

Fig. 8. First-order kinetics of MB photocatalytic degradation versus time without catalyst and in the presence of SiNWs and Bi@SiNWs under (a) UV light irradiation and (b) sunlight irradiation. The optimum rate constant (c) without catalyst and in the presence of SiNWs and Bi@SiNWs under UV and sunlight irradiation.

and holes during photocatalysis process have enough activity, different types of active species, namely superoxide radicals ($O_2^{\bullet-}$), hydroxyl radicals ($OH^{\bullet}$), hydrogen peroxide (H_2O_2), and singlet oxygen ($^1O_2{}^{\bullet}$) could be generated (Pichat, 2013; Li et al., 2013; Kobkeatthawin et al., 2022). Besides, for bismuth-based host materials in aqueous systems, it is found that a soluble species of Bi^{3+} is the most common and stable ionic form of bismuth and it is often used as an activator or sensitizer. This latter can absorb light and then triggers the subsequent formation of the required radicals (Riente et al., 2021). Herein, when the highly light-absorptive Bi@SiNWs material is irradiated with sunlight or UV light energy larger or equivalent than its band-gap ($h\nu \geq E_g$), an electron–hole (e^-/h^+) pair is produced and thereafter separated. Herein, the transport pathway of photo-generated electrons was established from the conduction band (CB) of Si toward the outer semimetal Bi nanoparticles. Indeed, the difference in the Fermi levels between semiconductor and metal can introduce the Schottky barrier between them, leading to the transfer of the e^- from the CB to the metal (Ghosh et al., 2018; Kiran et al., 2021).

Hence, the widespread BiNPs facilitated the carrier separation that effectively reduced the e^-/h^+ recombination. The released electrons can react with dissolved oxygen to form superoxide radicals ($O_2^{\bullet-}$) thus initiating actively the degradation of MB dyes as long as the photocatalysts were excited under light illumination. These highly oxidative species further reacts with water or hydroxide ions (H_2O/OH^-) to form mainly hydroxyl radicals ($OH^{\bullet}$) which can easily attack MB molecules to produce carbon dioxide (CO_2) and water (H_2O). Apart from that, the photogenerated holes can readily react with water or hydroxide ions (H_2O/OH^-) to yield mainly hydroxyl radicals ($OH^{\bullet}$), which offer another pathway promoting the efficient MB degradation.

This mechanism is shown in Fig. 9 and could be well elucidated using the following chemical Eqs. (8)–(14):

$$Bi@SiNWs + h\nu \rightarrow e^- + h^+ \quad (8)$$

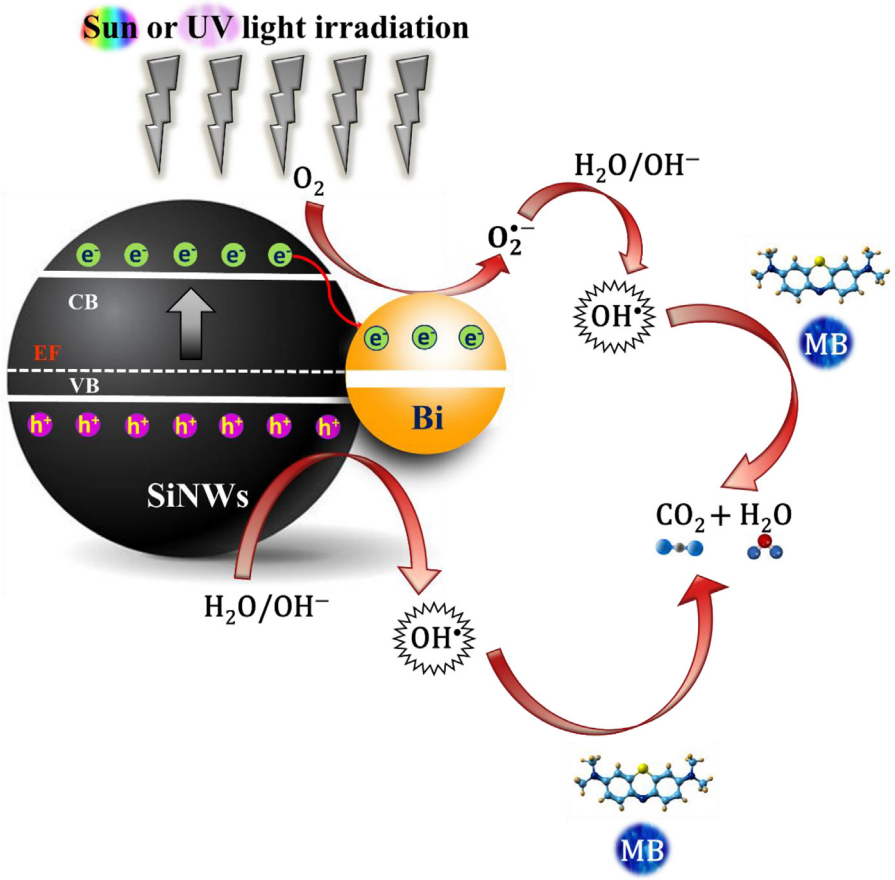

Fig. 9. Schematic illustration for the photocatalytic mechanism on MB dye degradation using Bi@SiNWs photocatalyst.

$$e^- + O_2 \Rightarrow O_2^{\bullet -} \quad (9)$$

$$O_2^{\bullet -} + H_2O \Rightarrow OH^{\bullet} + HO_2^- \quad (10)$$

$$O_2^{\bullet -} + OH^- + 2h^+ \Rightarrow OH^{\bullet} + O_2 \quad (11)$$

$$h^+ + H_2O \Rightarrow OH^{\bullet} + H^+ \quad (12)$$

$$h^+ + OH^- \Rightarrow OH^{\bullet} \quad (13)$$

$$OH^{\bullet} + MB \Rightarrow CO_2 + H_2O \quad (14)$$

Conclusion

In summary, extensive investigations of Bi modified SiNWs new photocatalyst are performed to remarkably improve the photo-degradation performances of MB dye under both UV and solar irradiations. SiNWs were produced via the 2-Ag-ACE technique, whereas BiNPs were coated throughout the vertically aligned wires by thermal evaporation. The resulting Bi@SiNWs nanocomposite morphology, elemental composition, structure, and crystallinity properties were characterized, confirming its successful manufacture. The systematic studies by reflectance, transmittance, absorption coefficient, absorbance and optical band-gap provided evidence for outstanding SiNWs and Bi@SiNWs optical properties. It has been shown that robust light-absorbance to above 97% (over the visible wavelength region) can be achieved by Bi@SiNWs. Moreover, the synergistic effect between the plasmonic BiNPs co-catalyst and the pure optically-active SiNWs showed enhanced photocatalytic activity. Within 120 min, up to 89% MB can be decomposed in sunlight. Interestingly, the recycling tests asserted the excellent photo-stability and reusability of the Bi@SiNWs composite photocatalyst. Ultimately, a plausible mechanism for the photocatalytic degradation of MB over Bi@SiNWs was thoroughly proposed. Our findings strongly attest to the great potential of Bi@SiNWs as a potent photocatalyst for MB degradation. All these gains can further promote using that new class of plasmonic photocatalyst in dye detoxification and other environment-related applications.

CRediT authorship contribution statement

Mariem Naffeti: Conceptualization, Data curation, Formal analysis, Funding acquisition, Investigation, Methodology, Resources, Software, Validation, Visualization, Writing – original draft, Writing – review & editing. **Mohamed Ali Zaïbi:** Conceptualization, Data curation, Formal analysis, Project administration, Supervision, Validation, Visualization, Writing – review & editing. **Chayma Nefzi:** Conceptualization, Methodology, Investigation, Validation, Visualization. **Alejandro Vidal García-Arias:** Investigation, Project administration, Software, Validation. **Radhouane Chtourou:** Investigation, Project administration, Resources, Software, Supervision, Validation, Writing – review & editing. **Pablo Aitor Postigo:** Conceptualization, Formal analysis, Funding acquisition, Investigation, Methodology, Project administration, Resources, Supervision, Validation, Visualization, Writing – review & editing.

Declaration of competing interest

The authors declare that they have no known competing financial interests or personal relationships that could have appeared to influence the work reported in this paper.

Data availability

Data will be made available on request.

Acknowledgments

M. Naffeti and P.A. Postigo acknowledge the service from the X-SEM Laboratory at IMN and funding from CSIC under i-COOP+ 2020 program (COOPA20431), Spain.

Appendix A. Supplementary data

Supplementary material related to this article can be found online at https://doi.org/10.1016/j.eti.2023.103133.

References

Al-Mamun, M.R., Kader, S., Islam, M.S., Khan, M.Z.H., 2019. Photocatalytic activity improvement and application of UV-tio2 photocatalysis in textile wastewater treatment: A review. J. Environ. Chem. Eng. 7 (5), 103248. http://dx.doi.org/10.1016/j.jece.2019.103248.

Babu, B., Cho, M., Byon, C., Shim, J., 2018. One pot synthesis of Ag-SnO_2 quantum dots for highly enhanced sunlight-driven photocatalytic activity. J. Alloys Compd. 731, 162–171. http://dx.doi.org/10.1016/j.jallcom.2017.10.011.

Benabdallah, I., Boujnah, M., El Kenz, A., Benyoussef, A., Abatal, M., Bassam, A., 2018. Lead-free perovskite based bismuth for solar cells absorbers. J. Alloys Compd. http://dx.doi.org/10.1016/j.jallcom.2018.09.332.

Brahiti, N., Hadjersi, T., Amirouche, S., Menari, H., ElKechai, O., 2018. Photocatalytic degradation of cationic and anionic dyes in water using hydrogen-terminated silicon nanowires as catalyst. Int. J. Hydrogen Energy 43 (24), 11411–11421. http://dx.doi.org/10.1016/j.ijhydene.2018.02.141.

Brahiti, N., Hadjersi, T., Menari, H., Amirouche, S., El Kechai, O., 2015. Enhanced photocatalytic degradation of methylene blue by metal-modified silicon nanowires. Mater. Res. Bull. 62, 30–36. http://dx.doi.org/10.1016/j.materresbull.2014.11.007.

Chaliyawala, H.A., Ray, A., Pati, R.K., Mukhopadhyay, I., 2017. Strong light absorption capability directed by structured profile of vertical Si nanowires. Opt. Mater. 73, 449–458. http://dx.doi.org/10.1016/j.optmat.2017.08.049.

Dong, F., Xiong, T., Sun, Y., Zhao, Z., Zhou, Y., Feng, X., Wu, Z., 2014. A semimetal bismuth element as a direct plasmonic photocatalyst. Chem. Commun. 50 (72), 10386–10389. http://dx.doi.org/10.1039/c4cc02724h.

Ensafi, A.A., Abarghoui, M.M., Rezaei, B., 2017. Metal (Ni and Bi) coated porous silicon nanostructure, high-performance anode materials for lithium ion batteries with high capacity and stability. J. Alloys Compd. 712, 233–240. http://dx.doi.org/10.1016/j.jallcom.2017.04.10.

Eskizeybek, V., Sarı, F., Gülce, H., Gülce, A., Avcı, A., 2012. Preparation of the new polyaniline/ZnO nanocomposite and its photocatalytic activity for degradation of methylene blue and malachite green dyes under UV and natural sun lights irradiations. Appl. Catal. B 119–120, 197–206. http://dx.doi.org/10.1016/j.apcatb.2012.02.03.

Gao, T., Wen, X., Xie, T., Han, N., Sun, K., Han, L., Wang, H., Zhang, Y., Kuang, Y., Sun, X., 2019. Morphology effects of bismuth catalysts on electroreduction of carbon dioxide into formate. Electrochim. Acta http://dx.doi.org/10.1016/j.electacta.2019.03.066.

García, C.R., Diaz-Torres, L.A., Oliva, J., Romero, M.T., Salas, P., 2016. Photocatalytic activity and optical properties of blue persistent phosphors under UV and solar irradiation. Int. J. Photoenergy 2016, 1–8. http://dx.doi.org/10.1155/2016/1303247.

Ghosh, R., Ghosh, J., Das, R., Mawlong, L.P.L., Paul, K.K., Giri, P.K., 2018. Multifunctional Ag nanoparticle decorated si nanowires for sensing, photocatalysis and light emission applications. J. Colloid Interface Sci. 532, 464–473. http://dx.doi.org/10.1016/j.jcis.2018.07.123.

Ghosh, R., Giri, P.K., 2016. Silicon nanowire heterostructures for advanced energy and environmental applications: a review. Nanotechnology 28 (1), 012001. http://dx.doi.org/10.1088/0957-4484/28/1/012001.

Hammouche, J., Daoudi, K., Columbus, S., Ziad, R., Ramachandran, K., Gaidi, M., 2021. Structural and morphological optimization of Ni doped ZnO decorated silicon nanowires for photocatalytic degradation of methylene blue. Inorg. Chem. Commun. 131, 108763. http://dx.doi.org/10.1016/j.inoche.2021.108763.

Hsiao, P.-H., Li, T.-C., Chen, C.-Y., 2019. ZnO/Cu2O/Si nanowire arrays as ternary heterostructure-based photocatalysts with enhanced photodegradation performances. Nanoscale Res. Lett. 14 (1), http://dx.doi.org/10.1186/s11671-019-3093-9.

Hsiao, P.-H., Timjan, S., Kuo, K.-Y., Juan, J.-C., Chen, C.-Y., 2021. Optical management of CQD/AgNP@SiNW arrays with highly efficient capability of dye degradation. Catalysts 11, 399. http://dx.doi.org/10.3390/catal11030399.

Hu, T., Liu, Q., Gao, T., Dong, K., Wei, G., Yao, J., 2018. Facile preparation of tannic acid–poly(vinyl alcohol)/sodium alginate hydrogel beads for methylene blue removal from simulated solution. ACS Omega 3 (7), 7523–7531. http://dx.doi.org/10.1021/acsomega.8b00577.

Hung, Y.-J., Lee, S.-L., Wu, K.-C., Tai, Y., Pan, Y.-T., 2011. Antireflective silicon surface with vertical-aligned silicon nanowires realized by simple wet chemical etching processes. Opt. Express 19 (17), 15792. http://dx.doi.org/10.1364/oe.19.015792.

Hutagalung, S.D., Fadhali, M.M., Areshi, R.A., Tan, F.D., 2017. Optical and electrical characteristics of silicon nanowires prepared by electroless etching. Nanoscale Res. Lett. 12 (1), http://dx.doi.org/10.1186/s11671-017-2197-3.

Ibrahim, S., Bonnet, P., Sarakha, M., Caperaa, C., Monier, G., Bousquet, A., 2019. Tailoring the structural and optical properties of bismuth oxide films deposited by reactive magnetron sputtering for photocatalytic application. Mater. Chem. Phys. 122580. http://dx.doi.org/10.1016/j.matchemphys.2019.122580.

Kashyap, V., Kashyap, V., Goyal, N., Saxena, K., 2021a. Fabrication and characterization of silicon nanowires with MACE method to influence the optical properties. Mater. Today: Proc. http://dx.doi.org/10.1016/j.matpr.2021.02.814.

Kashyap, V., Kumar, C., Chaudhary, N., Goyal, N., Saxena, K., 2021b. Comparative study of quantum confinements effect present in Silicon Nanowires using absorption and Raman spectroscopy. Opt. Mater. 121, 111538. http://dx.doi.org/10.1016/j.optmat.2021.111538.

Kiran, T., Parveez Ahmed, H.M., Shahina Begum, N., Manjunatha, K.G., 2021. Sun light driven photocatalytic performance of ag decorated TiO2 nanocomposite thin films by sol gel method. Mater. Today: Proc. 46, 5948–5952. http://dx.doi.org/10.1016/j.matpr.2020.11.385.

Kobkeatthawin, T., Trakulmututa, J., Amornsakchai, T., Kajitvichyanukul, P., Smith, S.M., 2022. Identification of active species in photodegradation of aqueous imidacloprid over g-C_3N_4/TiO_2 nanocomposites. Catalysts 12, 120. http://dx.doi.org/10.3390/catal12020120.

Kong, Z., Li, L., Xue, Y., Yang, M., Li, Y.Y., 2019. Challenges and prospects for the anaerobic treatment of chemical-industrial organic wastewater: A review. J. Cleaner Prod. 231, 913–927. http://dx.doi.org/10.1016/j.jclepro.2019.05.233.

Li, Wenjuan, Li, Danzhen, Wang, Jinxiu, Shao, Yu, You, Jinmao, Teng, Fei, 2013. Exploration of the active species in the photocatalytic degradation of methyl orange under UV light irradiation. J. Mol. Catal. A: Chem. 380, 10–17. http://dx.doi.org/10.1016/j.molcata.2013.09.001.

Lian, S., Tsang, C.H.A., Kang, Z., Liu, Y., Wong, N., Lee, S.-T., 2011. Hydrogen-terminated silicon nanowire photocatalysis: Benzene oxidation and methyl red decomposition. Mater. Res. Bull. 46 (12), 2441–2444. http://dx.doi.org/10.1016/j.materresbull.2011.08.027.

Liang, C.-Z., Sun, S.-P., Li, F.-Y., Ong, Y.-K., Chung, T.-S., 2014. Treatment of highly concentrated wastewater containing multiple synthetic dyes by a combined process of coagulation/flocculation and nanofiltration. J. Membr. Sci. 469, 306–315. http://dx.doi.org/10.1016/j.memsci.2014.06.057.

Liao, F., Wang, T., Shao, M., 2015. Silicon nanowires: applications in catalysis with distinctive surface property. J. Mater. Sci., Mater. Electron. 26 (7), 4722–4729. http://dx.doi.org/10.1007/s10854-015-2949-8.

Lin, X., Li, S.H., Lu, K.Q., Tang, Z.R., Xu, Y.J., 2018. Constructing film composites of silicon nanowires@CdS quantum dot arrays with ameliorated photocatalytic performance. New J. Chem. 42, 14096–14103. http://dx.doi.org/10.1039/C8NJ02883D.

Mallorquí, Anna Dalmau, Alarcón-Lladó, Esther, Mundet, Ignasi Canales, Kiani, Amirreza, Demaurex, Bénédicte, De Wolf, Stefaan, Menzel, Andreas, Zacharias, Margrit, Fontcuberta i Morral, Anna, 2015. Field-effect passivation on silicon nanowire solar cells. Nano Res. 8 (2), 673–681. http://dx.doi.org/10.1007/s12274-014-0551-7.

Mehwish, H.M., Rajoka, M.S.R., Xiong, Y., Cai, H., Aadil, R.M., Mahmood, Q., He, Z., Zhu, Q., 2021. Green synthesis of a silver nanoparticle using moringa oleifera seed and its applications for antimicrobial and sun-light mediated photocatalytic water detoxification. J. Environ. Chem. Eng. 9 (4), 105290. http://dx.doi.org/10.1016/j.jece.2021.105290.

Naama, S., Hadjersi, T., Menari, H., Nezzal, G., Ahmed, L.B., Lamrani, S., 2016. Enhancement of the tartrazine photodegradation by modification of silicon nanowires with metal nanoparticles. Mater. Res. Bull. 76, 317–326. http://dx.doi.org/10.1016/j.materresbull.2015.12.046.

Naffeti, M., Postigo, P.A., Chtourou, R., Zaïbi, M.A., 2020a. Elucidating the effect of etching time key-parameter toward optically and electrically-active silicon nanowires. Nanomaterials 10 (3), 404. http://dx.doi.org/10.3390/nano10030404.

Naffeti, M., Postigo, P.A., Chtourou, R., Zaïbi, M.A., 2020b. Highly efficient silicon nanowire surface passivation by bismuth nano-coating for multifunctional Bi@SiNWs heterostructures. Nanomaterials 10, 1434. http://dx.doi.org/10.3390/nano10081434.

Nefzi, C., Beji, N., Souli, M., Mejri, A., Alleg, S., Kamoun-Turki, N., 2019. Effect of gamma-irradiation on optical, structural and electrical properties of In_2O_3: F thin films for photocatalysis application. Opt. Laser Technol. 112, 85–92. http://dx.doi.org/10.1016/j.optlastec.2018.11.010.

Pelepenko, L.E., Janini, A.C.P., Gomes, B.P.F.A., de Jesus-Soares, A., Marciano, M.A., 2022. Effects of bismuth exposure on the human kidney—A systematic review. Antibiotics 11, 1741. http://dx.doi.org/10.3390/antibiotics11121741.

Pichat, Pierre, 2013. Photocatalysis and Water Purification (From Fundamentals to Recent Applications) || Identification and Roles of the Active Species Generated on Various Photocatalysts. pp. 1–24. http://dx.doi.org/10.1002/9783527645404.ch1.

Rani, P., Kumar, V., Singh, P.P., Matharu, A.S., Zhang, W., Kim …, K.-H., Rawat, M., 2020. Highly stable AgNPs prepared via a novel green approach for catalytic and photocatalytic removal of biological and non-biological pollutants. Environ. Int. 143, 105924. http://dx.doi.org/10.1016/j.envint.2020.105924.

Riente, P., Fianchini, M., Llanes, P., et al., 2021. Shedding light on the nature of the catalytically active species in photocatalytic reactions using Bi2O3 semiconductor. Nature Commun. 12, 625. http://dx.doi.org/10.1038/s41467-020-20882-x.

Rosu, M.C., Coros, M., Pogacean, F., Magerusan, L., Socaci, C., Turza, A., Pruneanu, S., 2017. Azo dyes degradation using tio_2-pt/graphene oxide and tio2-pt/reduced graphene oxide photocatalysts under UV and natural sunlight irradiation. Solid State Sci. 70, 13–20. http://dx.doi.org/10.1016/j.solidstatesciences.2017.05.013.

Samsami, S., Mohamadi, M., Sarrafzadeh, M.H., Rene, E.R., Firoozbahr, M., 2020. Recent advances in the treatment of dye-containing wastewater from textile industries: Overview and perspectives. Process Saf. Environ. Prot. 143, 138–163. http://dx.doi.org/10.1016/j.psep.2020.05.034.

Saratale, G.D., Saratale, R.G., Cho, S.-K., Ghodake, G., Bharagava, R.N., Park ., Y., Shin, H.-S., 2020. Investigation of photocatalytic degradation of reactive textile dyes by Portulaca oleracea-functionalized silver nanocomposites and exploration of their antibacterial and antidiabetic potentials. J. Alloys Compd. 155083. http://dx.doi.org/10.1016/j.jallcom.2020.155083.

Shen, S., Guo, L., 2008. Growth of quantum-confined CdS nanoparticles inside Ti-MCM-41 as a visible light photocatalyst. Mater. Res. Bull. 43 (2), 437–446. http://dx.doi.org/10.1016/j.materresbull.2007.02.034.

Shi, J., Huang, W., Zhu, H., Xiong, J., Bei, H., Wei, X., Wang, S., 2020. Modified TiO_2 particles for heterogeneous photocatalysis under solar irradiation. Mater. Lett. 128472. http://dx.doi.org/10.1016/j.matlet.2020.128472.

Sudina, Lyudmila, Kolesnikov, Sergey, Minnikova, Tatiana, Kazeev, Kamil, Sushkova, Svetlana, Minkina, Tatiana, 2021. Assessment of ecotoxicity of the bismuth by biological indicators of soil condition. Eurasian J. Soil Sci. 10 (3), 236–242. http://dx.doi.org/10.18393/ejss.926759.

Sun, H.-T., Zhou, J., Qiu, J., 2014. Recent advances in bismuth activated photonic materials. Prog. Mater. Sci. 64, 1–72. http://dx.doi.org/10.1016/j.pmatsci.2014.02.002.

Swain, B.S., Swain, B.P., Hwang, N.M., 2011. Investigation of optical properties of core–shell silicon nanowires. Mater. Chem. Phys. 129 (3), 733–739. http://dx.doi.org/10.1016/j.matchemphys.2011.04.046.

Tang, C.-H., Chen, K.-Y., Chen, C.-Y., 2018. Solution-processed ZnO/Si based heterostructures with enhanced photocatalytic performance. New J. Chem. 42 (16), 13797–13802. http://dx.doi.org/10.1039/c8nj03015d.

Theerthagiri, J., Chandrasekaran, Sivaraman, Salla, Sunitha, Elakkiya, V., Senthil, R.A., Nithyadharseni, P., Maiyalagan, T., Micheal, Kavin, Ayeshamariam, A., Arasu, M. Valan, Al-Dhabi, Naif Abdullah, Kim, Hyun-Seok, 2018. Recent developments of metal oxide based heterostructures for photocatalytic applications towards environmental remediation. J. Solid State Chem. 267, 35–52. http://dx.doi.org/10.1016/j.jssc.2018.08.006.

Wang, M., Chen, J., Liao, X., Liu, Z., Zhang, J., Gao, L., Li, Y., 2014. Highly efficient photocatalytic hydrogen production of platinum nanoparticle-decorated SiC nanowires under simulated sunlight irradiation. Int. J. Hydrogen Energy 39 (27), 14581–14587. http://dx.doi.org/10.1016/j.ijhydene.2014.07.068.

Wang, S., Tang, S., Gao, H., Chen, X., Liu, H., Yu ., C., Yang, H., 2021. Microstructure, optical, photoluminescence properties and the intrinsic mechanism of photoluminescence and photocatalysis for the BaTiO3, $BaTiO_3/TiO_2$ and BaTiO3/TiO2/CeO2 smart composites. Opt. Mater. 118, 111273. http://dx.doi.org/10.1016/j.optmat.2021.111273.